The Mechanism for Water Exchange in $[UO_2(H_2O)_5]^{2+}$ and $[UO_2(oxalate)_2(H_2O)]^{2-}$, as Studied by Quantum Chemical Methods

Valérie Vallet,*,†,‡ Ulf Wahlgren,† Bernd Schimmelpfennig,§ Zoltán Szabó,⊥ and Ingmar Grenthe*,⊥

Contribution from the Institute of Physics, Stockholm University, P.O. Box 6730, S-11385 Stockholm, Sweden, Laboratoire de Physique Quantique, Université Paul Sabatier, F-31062 Toulouse, France, Theoretical Chemistry, Department of Biotechnology, Royal Institute of Technology (KTH), S-10044 Stockholm, Sweden, and Inorganic Chemistry, Department of Chemistry, Royal Institute of Technology (KTH), S-10044 Stockholm, Sweden

Received April 3, 2001

Abstract: The mechanisms for the exchange of water between $[UO_2(H_2O)_5]^{2+}$, $[UO_2(oxalate)_2(H_2O)]^{2-}$, and water solvent along dissociative (*D*), associative (*A*) and interchange (*I*) pathways have been investigated with quantum chemical methods. The choice of exchange mechanism is based on the computed activation energy and the geometry of the identified transition states and intermediates. These quantities were calculated both in the gas phase and with a polarizable continuum model for the solvent. There is a significant and predictable difference between the activation energy of the gas phase and solvent models: the energy barrier for the *D*-mechanism increases in the solvent as compared to the gas phase, while it decreases for the *A*- and *I*-mechanisms. The calculated activation energy, $\Delta U^{\ddagger}$, for the water exchange in $[UO_2(H_2O)_5]^{2+}$ is 74, 19, and 21 kJ/mol, respectively, for the *D*-, *A*-, and *I*-mechanisms in the solvent, as compared to the experimental value $\Delta H^{\ddagger} = 26 \pm 1$ kJ/mol. This indicates that the *D*-mechanism for this system can be ruled out. The energy barrier between the intermediates and the transition states is small, indicating a lifetime for the intermediate $\approx 10^{-10}$ s, making it very difficult to distinguish between the *A*- and *I*-mechanisms experimentally. There is no direct experimental information on the rate and mechanism of water exchange in $[UO_2(oxalate)_2(H_2O)]^{2-}$ containing two bidentate oxalate ions. The activation energy and the geometry of transition states and intermediates along the *D*-, *A*-, and *I*-pathways were calculated both in the gas phase and in a water solvent model, using a single-point MP2 calculation with the gas phase geometry. The activation energy, $\Delta U^{\ddagger}$, in the solvent for the *D*-, *A*-, and *I*-mechanisms is 56, 12, and 53 kJ/mol, respectively. This indicates that the water exchange follows an associative reaction mechanism. The geometry of the *A*- and *I*-transition states for both $[UO_2(H_2O)_5]^{2+}$ and $[UO_2(oxalate)_2(H_2O)]^{2-}$ indicates that the entering/leaving water molecules are located outside the plane formed by the spectator ligands.

Introduction

The coordination chemistry of U(VI) differs from that of the d-transition and main-group elements in that all labile ligands are located in a plane perpendicular to the linear UO_2-axis. There are a number of experimental investigations[1−3] of ligand exchange/substitution reactions on the UO_2^{2+} ion, but no prior theoretical studies of their intimate mechanisms, i.e. transition states and activation energies. Mechanistic information can be obtained from experimental rate laws and activation parameters,[2−4] and/or by using theoretical methods. In the present paper we will analyze exchange mechanisms for UO_2^{2+} complexes in solution using quantum chemical methods. They are based on the assumption that the calculated activation energy is sufficiently accurate to allow a choice between different mechanisms. The following factors must be considered:

1. The quality of the quantum chemical approximations: In the present case the calculations have been made at the HF/MP2 level. This approximation was tested in our previous paper[5] where a comparison of HF/MP2 and DFT/B3PW91 calculations showed only minor differences in energy and geometry. We have also tested B3LYP, which gives virtually the same result.

2. The quality of the solvent model used, in particular the approximations necessary to describe the second coordination sphere and the bulk solvent: These issues have been discussed in our previous paper[5] and also by other investigators[6−12] and are the reason we have used a shape adapted dielectric medium model.

3. The approximations required to compare the activation energy $\Delta U^{\ddagger}$, calculated by quantum chemistry at 0 K in a

† Stockholm University.
‡ Université Paul Sabatier.
§ Department of Biotechnology, Royal Institute of Technology.
⊥ Department of Chemistry, Royal Institute of Technology.

(1) Lincoln, S. F. *Pure Appl. Chem.* **1979**, *51*, 2059.
(2) Szabó, Z.; Glaser, J.; Grenthe, I. *Inorg. Chem.* **1996**, *35*, 2036.
(3) Szabó, Z.; Grenthe, I. *Inorg. Chem.* **1998**, *37*, 6214.
(4) Drljaca, A.; Hubbard, C. D.; van Eldik, R.; Asano, T.; Basilevsky, M. V.; le Noble, W. J. *Chem. Rev.* **1998**, *98*, 2167.
(5) Vallet, V.; Wahlgren, U.; Schimmelpfennig, B.; Moll, H.; Szabó, Z.; Grenthe, I. *Inorg. Chem.* **2001**, *40*, 3516.
(6) Rotzinger, F. P. *J. Am. Chem. Soc.* **1996**, *118*, 6760.
(7) Rotzinger, F. P. *J. Am. Chem. Soc.* **1997**, *119*, 5230.
(8) Rotzinger, F. P. *J. Phys. Chem. A* **1999**, *103*, 9345.
(9) Rotzinger, F. P. *J. Phys. Chem. A* **2000**, *104*, 6439.
(10) Kowall, T.; Caravan, P.; Bourgeois, H.; Helm, L.; Rotzinger, F. P.; Merbach, A. E. *J. Am. Chem. Soc.* **1998**, *120*, 6569.
(11) Rotzinger, F. P. *Helv. Chim. Acta* **2000**, *83*, 3006.
(12) Hartmann, M.; Clark, T.; van Eldik, R. *J. Phys. Chem. A* **1999**, *103*, 9899.

10.1021/ja015935+ CCC: $20.00
Published on Web 11/03/2001

Scheme 1

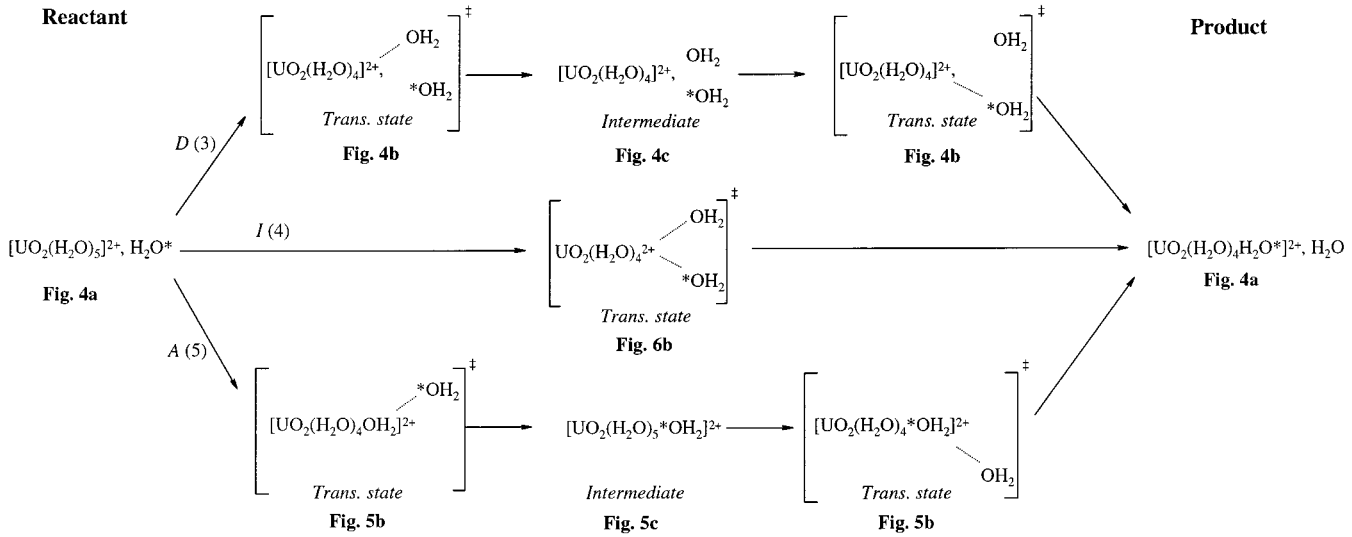

solvent, with the experimental activation enthalpy $\Delta H^{\ddagger}$ at 298 K: We will come back to this point in the discussion.

The procedures used to investigate exchange mechanisms will follow the path set by Rotzinger et al.[6−11] and Hartmann et al.[12,13] on d-transition and main-group elements. Their early studies have in general been made by using a gas phase model, an approximation that was justified by the good agreement between experimental values of $\Delta H^{\ddagger}$ and the theory based activation energy $\Delta U^{\ddagger}$. This agreement may be fortuitous; associative (*A*), dissociative (*D*), and interchange mechanisms (*I*) are affected in different, but predictable ways by the introduction of solvent effects. Rotzinger et al.[8−11] have recently used a model with a spherical solvent cavity for the geometry and a shape-adapted cavity for the calculation of energy. However, it is more appropriate to use a shape-adapted cavity[14] for both calculations, as demonstrated, for example, in our study of the geometry and energy of uranium(VI) fluoride and hydroxide complexes;[5] it seems likely that this is also the case for kinetic parameters.

In a previous study[15] we measured the rates and activation parameters for the exchange between $[UO_2(H_2O)_5]^{2+}$ and bulk water and suggested a dissociative reaction mechanism. This proposal was based on geometric considerations; four-coordinated U(VI) complexes with unidentate ligands are more common than six-coordinated, and on the calculated energy in the gas phase for the reactions

$$[UO_2(H_2O)_5]^{2+} \rightarrow [UO_2(H_2O)_4]^{2+}\cdot(H_2O) \qquad \Delta U = 41.0 \text{ kJ/mol} \quad (1)$$

$$[UO_2(H_2O)_5]^{2+}\cdot(H_2O) \rightarrow [UO_2(H_2O)_6]^{2+} \qquad \Delta U = 93.7 \text{ kJ/mol} \quad (2)$$

that favor the dissociative reaction 1; the water outside the brackets is located in the second coordination sphere. In the present study we scrutinize this conclusion using a quantum chemical model that includes the solvent.

Observations on d-transition and main-group elements indicate an increased lability of water in the first coordination sphere when part of it is replaced by other ligands.[16] On the other hand, we have strong experimental indications that the water exchange in complexes such as $[UO_2(\text{oxalate})F_2(H_2O)]^{2-}$ is slow.[17] We will investigate if the different behavior of the uranyl complexes is a result of changes in the activation energy and/or the substitution mechanism.

The UO_2^{2+} center exerts a very strong inductive effect on coordinated ligands, as indicated, e.g., by the large increase in dissociation constant for glycolate, from approximately 10^{-17} in free $HOCH_2COO^-$ to $10^{-3.64}$ when coordinated,[18] and a substantial change in chemical reactivity of coordinated organic substrates.[19] Information on the structure and energy barriers along the reaction coordinate is important in understanding observations of this type and exploiting them in chemical reactions.

The intimate mechanisms for water exchange in $[UO_2(H_2O)_5]^{2+}$ and $[UO_2(\text{oxalate})_2(H_2O)]^{2-}$ were studied both in gas phase and solution, in the latter case using a conductor-like polarizable continuum (CPCM) solvent model with a cavity adapted to the geometry of the solute; from these results we will make an attempt to draw some general conclusions along the lines indicated above.

Methods

Model Reactions. The experimental data refer to water exchange between the first coordination sphere and the bulk solvent. The rate of exchange between the second coordination sphere and the bulk solvent is known to be very fast and the rate-determining step is thus the exchange between the first and second coordination spheres; this is the focus of our enquiry.

It is not possible to include a complete second coordination sphere in the models. We therefore restricted it to a single water molecule using the model reactions given in Schemes 1 and 2. *D*, *I*, and *A* denote dissociative, interchange, and associative exchange mechanisms, respectively; the designations will be referred to in the following text. The effect of the solvent is described by using the CPCM[14,20] model as implemented in Gaussian98.[21] It turned out to be both difficult and costly to optimize the geometry of the oxalate complexes in a CPCM

(13) Hartmann, M.; Clark, T.; van Eldik, R. *J. Am. Chem. Soc.* **1997**, *119*, 7843.
(14) Barone, V.; Cossi, M. *J. Phys. Chem. A* **1998**, *102*, 1995.
(15) Farkas, I.; Bányai, I.; Szabó, Z.; Wahlgren, U.; Grenthe, I. *Inorg. Chem.* **2000**, *39*, 799.
(16) Phillips, B. L.; Casey, W. H.; Neugebauer Crawford, S. *Geochim. Cosmochim. Acta* **1997**, *61*, 3041.
(17) Szabó, Z.; Aas, W.; Grenthe, I. *Inorg. Chem.* **1997**, *36*, 5369.
(18) Szabó, Z.; Grenthe, I. *Inorg. Chem.* **2000**, *39*, 5036.
(19) van Axel Castelli, V.; Dalla Cort, A.; Mandolini, L.; Reinhoudt, D. N.; Sciaffino, L. *Chem. Eur. J.* **2000**, *6*, 1193.
(20) Klamt, A.; Schüürmann, G. *J. Chem. Soc., Perkin. Trans.* **1993**, *2*, 799.

Scheme 2

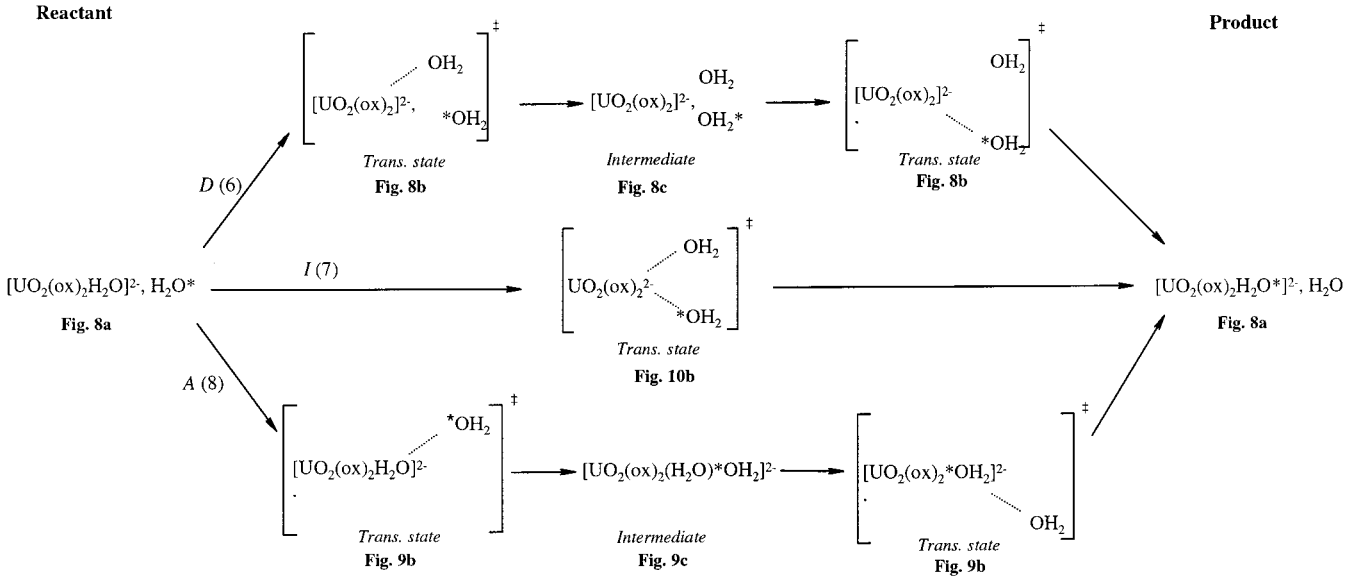

model. For these systems we instead estimated the correlation and solvent effects from single-point calculations in the gas phase and in the solvent using the gas phase geometry. On the basis of the results for the uranyl aqua ion, the difference in energy in the solvent between a single-point calculation using the gas phase geometry and a complete optimization is small, cf. Table 4 and the Discussion.

The *D*- and *A*-mechanisms have transition states that are followed by intermediates with coordination numbers four and six. The *I*-mechanism describes a concerted pathway with a symmetric transition state, where the entering and leaving ligands are at equal distances from the reaction center. The preferred reaction mechanism for these elementary reactions is the one with the lowest activation energy.

Computational Details and Method for Identification of Transition States. The basis sets and effective core potentials used are the same as in a previous communication,[5] where also a description is given of different solvent models. The calculations in the gas phase and in the CPCM solvent have been made at the Hartree−Fock level for the geometry optimizations and at the MP2 level for energies, using Gaussian98.[21] In the CPCM model, the solute is embedded in a shape-adapted cavity defined by interlocking spheres centered on each solute atom or group and with standard UATM (United Atomic Topological Model)[22] radii. The electrostatic and nonelectrostatic terms are included in the solvation energy derivatives, allowing geometry optimization using gradients within the bulk model. In the gas phase calculations we computed the vibration frequencies using analytical second derivatives, whereas we used numerical second derivatives in the solvent model. The volume change of the CPCM cavity was used to estimate the activation volume $\Delta V^{\ddagger}$. The experimental value is an important mechanistic indicator; however, it is not straightforward to compare $\Delta V^{\ddagger}$(experimental) with $\Delta V^{\ddagger}$(CPCM) as discussed in a number of reviews.[4,23]

The geometry of the reactants, products, and transition states was optimized without symmetry constraints. The transition states were identified by a single imaginary frequency corresponding to the translation of the leaving/entering ligands. Technically, the potential surface was explored by incremental stretching of the selected $U-OH_2$ bond starting either from the ground-state configuration of the different complexes or from the intermediates. This distance was then fixed while all the other internal coordinates were re-optimized. The constrained optimization was performed for different values of the $U-OH_2$ distance until an imaginary mode was found. At this point, we located the transition state by following the appropriate negative eigenmode. Occasionally, the automatic optimization procedure in Gaussian98 failed and in these cases we carried out the calculations by making incremental changes of the $U-OH_2$ distance until the transition state was located. For the *D*-mechanism we also tested a simplified model without a second coordination sphere

$$[UO_2(H_2O)_5]^{2+} \rightarrow \{[UO_2(H_2O)_4\cdots H_2O]^{2+}\}^{\ddagger} \rightarrow [UO_2(H_2O)_4]^{2+}\cdot(H_2O) \quad (9)$$

$$[UO_2(ox)_2(H_2O)]^{2-} \rightarrow \{[UO_2(ox)_2\cdots(H_2O)]^{2-}\}^{\ddagger} \rightarrow [UO_2(ox)_2]^{2-}\cdot(H_2O) \quad (10)$$

We used the permittivity of water, $\epsilon_r = 80$, for the dielectric continuum.

The intimate mechanism was assumed to be the one with the lowest activation energy. It turned out that the agreement between the calculated activation energy, $\Delta U^{\ddagger}$(0K), and the experimental value, $\Delta H^{\ddagger}$(298K), was within the expected accuracy of the theoretical methods used.

Results

$[UO_2(H_2O)_5]^{2+}\cdot(H_2O)$ was used as a starting structure to explore the *D*-, *I*-, and *A*-mechanisms, cf. Figure 1. The results for the water exchange in $[UO_2(H_2O)_5]^{2+}$ are given in Tables 1−4, in Figures 1−6, and as Supporting Information. The latter contains information on the total energy and coordinates of all species and all figures not shown in the main text.

$[UO_2(H_2O)_5]^{2+}$, $[UO_2(H_2O)_4]^{2+}$, and $[UO_2(H_2O)_6]^{2+}$. (a) Structure and Thermodynamics. The bond distances in $[UO_2(H_2O)_5]^{2+}$, Figure 2, are in fair agreement with experimental EXAFS structure data from solution[24] considering the systematic errors due to the theoretical approach used.[5,24] Inclusion of a solvent model in general results in a shortening

(21) Frisch, M. J.; Trucks, G. W.; Schlegel, H. B.; Scuseria, G. E.; Robb, M. A.; Cheeseman, J. R.; Zakrzewski, V. G.; Montgomery, J. A.; Stratmann, R. E.; Burant, J. C.; Dapprich, S.; Millam, J. M.; Daniels, A. D.; Kudin, K. N.; Strain, M. C.; Farkas, O.; Tomasi, J.; Barone, V.; Cossi, M.; Cammi, R.; Mennucci, B.; Pomelli, C.; Adamo, C.; Clifford, S.; Ochterski, J.; Petersson, G. A.; Ayala, P. Y.; Cui, Q.; Morokuma, K.; Malick, D. K.; Rabuck, A. D.; Raghavachari, K.; Foresman, J.; Cioslowski, J. B.; Ortiz, J. V.; Stefanov, B. B.; Liu, G.; Liashenko, A.; Piskorz, P.; Komaromi, I.; Gomperts, R.; Martin, R. L.; Fox, D. J.; Keith, T.; Al-Laham, M. A.; Peng, C. Y.; Nanayakkara, A.; Gonzalez, C.; Challacombe, M.; Gill, P. M. W.; Johnson, B. G.; Chen, W.; Wong, M. W.; Andres, J. L.; Head-Gordon, M.; Replogle, E. S.; Pople, J. A. *Gaussian 98*, Revision A.9; Gaussian, Inc.: Pittsburgh, PA 1998.

(22) Barone, V.; Cossi, M.; Tomasi, J. *J. Chem. Phys.* **1997**, *107*, 3210.

(23) Merbach, A. E. *Pure Appl. Chem.* **1982**, *54*, 1479.

(24) Wahlgren, U.; Moll, H.; Grenthe, I.; Schimmelpfennig, B.; Maron, L.; Vallet, V.; Gropen, O. *J. Phys. Chem. A* **1999**, *103*, 8257.

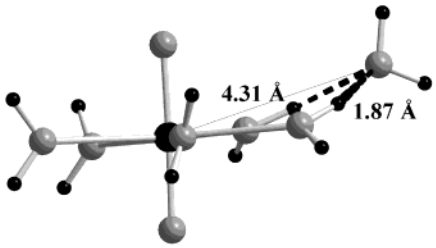

Figure 1. Perspective view of the reactant $[UO_2(H_2O)_5]^{2+}\cdot(H_2O)$ for the *D*-, *A*-, and *I*-mechanisms in solvent. The uranium atom and the hydrogen atoms are black and the oxygen atoms medium gray.

of the $U-OH_2$ bond distances with 0.07 Å as compared to the gas-phase value, which agrees well with the observations of Spencer et al.[25] and Tsushima et al.[26] An extensive discussion has recently been given by Mennucci et al.[27] The experimental solution structure data give no information on the orientation of the water molecules, only on the average bond distance and its distribution, which is approximately 0.08 Å around the average as estimated from the Debye−Waller factors from the EXAFS data.[24] The energy difference between different orientations of the water molecules is small, estimated in a previous theoretical study[24] at less than 2 kJ/mol. This indicates that the complex $[UO_2(H_2O)_5]^{2+}$ in solution is a mixture of various conformers in rapid equilibrium.

Stable structures, with only real vibration frequencies, have been found for $[UO_2(H_2O)_4]^{2+}$ (Supporting Information, S1), $[UO_2(H_2O)_5]^{2+}$ (Figure 2), and $[UO_2(H_2O)_6]^{2+}$ (Figure 3), the latter only in the solvent. The $[UO_2(H_2O)_6]^{2+}$ structure is of particular interest because it may be an intermediate in an associative pathway. Hay et al.[28] found two stable isomers in the gas phase using B3LYP and large core ECPs, one clearly six-coordinated with U−water bond lengths between 2.52 and 2.61 Å, and the other with five water molecules in the first shell and the sixth hydrogen bonded in the second sphere. The latter structure was found to be 16.9 kJ/mol more stable than the six-coordinated complex. However, all our attempts to find a stable six-coordinated ion failed in the gas phase: one water molecule always left the first hydration sphere to a bridging hydrogen bond position in the second sphere, cf. Figure S2. This difference might depend on the choice of basis set, as observed on other systems,[13] or on the choice of computational model. The intermediate $[UO_2(H_2O)_6]^{2+}$ is stable in the solvent with a very distorted structure similar to the one found by Hay et al.;[28] there are four water molecules located close to the equatorial plane at a distance of 2.49 Å, while the remaining ones are located above and below the plane, at 2.65 Å from U, cf. Figure 3. The O−U−O angle is 171°, with a bending energy of 9 kJ/mol, which is smaller than the bond energy of a water molecule in the second coordination sphere.

The relative energy of complexes with different numbers of coordinated water ligands is not the same in the gas-phase and solvent models.[24−26,28] However, the five-coordinated complex is always the most stable one. The energy change ΔU for reactions 11 and 12 in the CPCM solvent is given in Table 4 and favors the associative pathway, cf. eq 12.

$$[UO_2(H_2O)_5]^{2+}\cdot(H_2O) \rightarrow [UO_2(H_2O)_4]^{2+}\cdot(H_2O)_2 \qquad \Delta U = 62 \text{ kJ/mol} \quad (11)$$

$$[UO_2(H_2O)_5]^{2+}\cdot(H_2O) \rightarrow [UO_2(H_2O)_6]^{2+} \qquad \Delta U = 16 \text{ kJ/mol} \quad (12)$$

However, in the gas phase the *D*-pathway is favored with about 40 kJ/mol as compared to the *A*-pathway, as discussed below, cf. Table 2. This latter result is in contrast to that obtained in a previous study in the gas phase,[24] cf. eqs 1 and 2, where we used symmetry constraints when calculating the energy of the different structures.

(b) The Dissociative Mechanism. The transition state $\{[UO_2(H_2O)_4\cdots(H_2O)]^{2+}\cdot(H_2O)\}^{\ddagger}$ and the intermediate $[UO_2(H_2O)_4]^{2+}\cdot(H_2O)_2$ for the *D*-mechanism in the solvent are shown in Figure 4b,c. The spectator ligands in the transition state are located in the plane perpendicular to the "yl" axis, at distances close to those in the ground state. One of the symmetry equivalent ligands in the intermediate is located above and the other below the coordination plane, cf. Table 3 and Figure 4c. The activation energy $\Delta U^{\ddagger}$ and the activation volume $\Delta V^{\ddagger}$ obtained with use of the CPCM model are 74 kJ/mol and +4.6 cm^3/mol, respectively cf. Table 4. The activation energy in the gas phase is 46 kJ/mol cf. Table 2, indicating the uncertainty to be expected when making mechanistic deductions for solutions using a gas-phase model. Equations 3 (Scheme 1) and 9, the latter without a second coordination sphere, give essentially the same results for the geometry, but not for the energy, cf. Tables 2 and 4 and Figure S3.

(c) The Associative Mechanism. Since the six-coordinated complex is unstable in the gas phase, the associative mechanism could only be studied in the CPCM model. It was modeled using eq 5 (Scheme 1) by stretching one of the $U-OH_2$ bonds in the intermediate $[UO_2(H_2O)_6]^{2+}$, cf. Figure 5c. We found $\Delta U^{\ddagger} =$ 19 kJ/mol and $\Delta V^{\ddagger} = -3.0$ cm^3/mol, cf. Table 4. The geometry of the transition state is shown in Figure 5b, with bond distances given in Table 3. The spectator ligands are also in this case in (or close to) the plane perpendicular to the "yl" axis. The entering and leaving ligands are located above and below this plane, with the angle $H_2O_{ent}-U-H_2O_{leav}$ equal to 61.8°. The energy difference between the transition state and the following intermediate is only 3 kJ/mol; the geometry of the latter is close to that of the transition state for the interchange mechanism in the gas phase.

(d) The Interchange Mechanism. For technical reasons, the transition state could only be identified in the gas phase. The fastest way to search for it was to increase the two symmetry related $U-H_2O$ distances in $[UO_2(H_2O)_6]^{2+}$. The activation energy $\Delta U^{\ddagger}$ in the gas phase is equal to 38 kJ/mol. The transition state, Figure 6b, has C_2 symmetry and a geometry that is close to the intermediate found for the *A*-mechanism in solution, cf. Figures 5c and 6b.

An estimate of the activation energy for the *I*-mechanism in solution was made by a single-point MP2 calculation in the solvent using the gas-phase geometry. This activation energy, 21 kJ/mol, cf. Table 4, is very close to the energy of the *A*-intermediate, 16 kJ/mol, as are their geometries, cf. Tables 1 and 3.

(e) Conclusion. The activation energy for the *A*/*I*-mechanisms is much lower than that for *D*, indicating that the latter can be ruled out as a pathway for water exchange in $[UO_2(H_2O)_5]^{2+}$. The *A*- and *I*-pathways are in this case so similar that they cannot be distinguished with the methods we have used.

The $[UO_2(oxalate)_2(H_2O)]^{2-}$ System. The water exchange in $[UO_2(oxalate)_2(H_2O)]^{2-}$ was studied in order to explore how

(25) Spencer, S.; Gagliardi, L.; Handy, N. C.; Ioannou, A. G.; Skylaris, C.-K.; Willets, A. *J. Phys. Chem. A* **1999**, *103*, 1831.
(26) Tsushima, S.; Suzuki, A. *J. Mol. Struct.* **2000**, *529*, 21.
(27) Mennucci, B.; Martínez, J. M.; Tomasi, J. *J. Phys. Chem. A* **2001**, *105*, 7287.
(28) Hay, P. J.; Martin, R. L.; Schreckenbach, G. *J. Phys. Chem. A* **2000**, *104*, 6259.

Table 1. Calculated Bond Distances and Point Group Assignment for the Species Participating in the Water Exchange Reaction[a]

chemical species	sym	figure	d(U−O) (Å)	$H_I\cdots O_{II}$ (Å)
$[UO_2(H_2O)_4]^{2+}$	D_{4h}		2.48, 2.48, 2.48, 2.48	
$[UO_2(H_2O)_5]^{2+}$ (reactant)	C_5		2.53	
$\{[UO_2(H_2O)_4\cdots(H_2O)]^{2+}\}^{\ddagger}$ (*D*)	C_1		2.46, 2.48, 2.48, 2.49, 3.40	2.06
$[UO_2(H_2O)_4]^{2+}\cdot(H_2O)$ (*D*-intermediate)	C_s		2.46, 2.46, 2.48, 2.48, 4.00	2.05, 2.05
$[UO_2(H_2O)_5]^{2+}\cdot(H_2O)$ (reactant)	C_s	Figure S2	2.52, 2.52, 2.54, 2.54, 2.54, 4.38	1.93, 1.93
$\{[UO_2(H_2O)_4\cdots(H_2O)]^{2+}\cdot(H_2O)\}^{\ddagger}$ (*D*)	C_1		2.45, 2.47, 2.47, 2.48, 3.52, 4.06	1.97, 2.03, 2.03
$[UO_2(H_2O)_4]^{2+}\cdot(H_2O)_2$ (*D*-intermediate)	C_{2h}		2.47, 2.47, 2.47, 2.47, 3.94, 3.94	2.07, 2.10, 2.07, 2.10
$\{[UO_2(H_2O)_4\cdots 2(H_2O)]^{2+}\}^{\ddagger}$ (*I*)	C_2	Figure 6b	2.54, 2.54, 2.54, 2.54, 2.79, 2.79	

[a] The geometry optimizations have been made without symmetry constraints at the HF level in the gas phase. H···O denotes the hydrogen bond distance between the water oxygen in the second coordination sphere and hydrogen atoms of the water in the first coordination sphere.

Table 2. HF and MP2 Energy Changes (ΔU, in kJ/mol) in the Gas Phase for *D*-, and *I*-Mechanisms for Water Exchange in $[UO_2(H_2O)_5]^{2+}$ [a]

chemical species	ΔU(SCF) (kJ/mol)	ΔU(MP2) (kJ/mol)
$[UO_2(H_2O)_5]^{2+}$ (reactant)	0	0
$\{[UO_2(H_2O)_4\cdots(H_2O)]^{2+}\}^{\ddagger}$(*D*)	31.9	37.0
$[UO_2(H_2O)_4]^{2+}\cdot(H_2O)$ (*D*-intermediate)	26.5	29.2
$[UO_2(H_2O)_5]^{2+}\cdot(H_2O)$ (reactant)	0	0
$\{[UO_2(H_2O)_4\cdots(H_2O)]^{2+},(H_2O)\}^{\ddagger}$(*D*)	39.1	45.7
$[UO_2(H_2O)_4]^{2+}\cdot(H_2O)_2$ (*D*-intermediate)	37.4	42.9
$\{[UO_2(H_2O)_4\cdots 2(H_2O)]^{2+}\}^{\ddagger}$(*I*)	38.1	38.1

[a] The experimental activation parameters are $\Delta H^{\ddagger} = 26 \pm 1$ kJ/mol and $\Delta S^{\ddagger} = -40 \pm 5$ J/(mol·K).

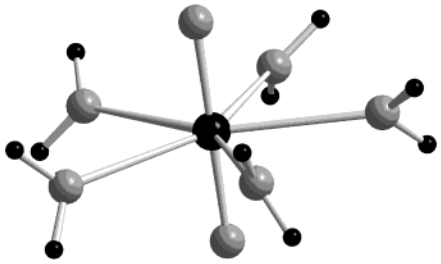

Figure 2. Dioxouranium(VI) aqua ion $[UO_2(H_2O)_5]^{2+}$ in solvent. The uranium atom and the hydrogen atoms are black and the oxygen atoms medium gray.

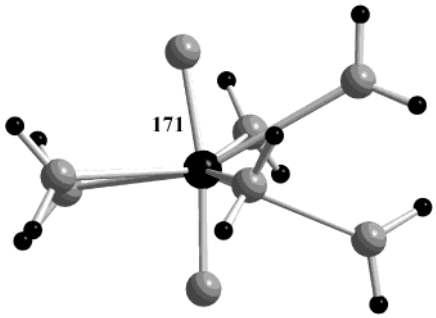

Figure 3. Perspective view of the hexacoordinated intermediate $[UO_2(H_2O)_6]^{2+}$ formed in the *A*-mechanism in the solvent. The uranium atom and the hydrogen atoms are black and the oxygen atoms medium gray.

different spectator ligands influence the activation energy and/or the mechanism for the water exchange. The water exchange was investigated both with the gas phase and CPCM models, in the latter case using a single-point MP2 calculation and the gas-phase geometry. The results of the quantum chemical calculations on the oxalate system are given in Tables 5 and 6, Figures 7−10, and the Supporting Information.

(a) Structure and Thermodynamics. The computed distance between uranium and oxygen in $[UO_2(oxalate)_2]^{2-}$ is 2.35−2.39 Å (Figure S4). The complex has a symmetry close to D_{2h}, which is a stable minimum with two planar oxalate groups in the equatorial plane. In $[UO_2(oxalate)_2(H_2O)]^{2-}$, Figure 7, the oxalate groups are slightly tilted with respect to the uranyl axis, resulting in a symmetry close to C_s. The U−O_{ox} distances are 2.36 and 2.42 Å and the U−water distance is 2.62 Å. The oxalate distances are in good agreement with X-ray data from solids[29] and EXAFS data from solution,[30] 2.38 Å, while the U−H_2O distance is 0.17 Å longer than the experimental value. Part of this, at least 0.07 Å, is due to the neglect of solvent effects in the geometry optimization, as discussed for the uranyl aqua ion. The energy change, ΔU, for reactions 13 and 14 favors the dissociative pathway in the gas phase and the associative pathway in the solvent, as was the case for the water exchange in the aqua ion.

$$[UO_2(oxalate)_2(H_2O)]^{2-}\cdot(H_2O) \rightarrow [UO_2(oxalate)_2]^{2-}\cdot(H_2O)_2 \quad (13)$$

$$\Delta U(\text{gas phase}) = 8 \text{ kJ/mol}; \Delta U(\text{CPCM}) = 54 \text{ kJ/mol}$$

$$[UO_2(oxalate)_2(H_2O)]^{2-}\cdot(H_2O) \rightarrow [UO_2(oxalate)_2(H_2O)_2]^{2-} \quad (14)$$

$$\Delta U(\text{gas phase}) = 25 \text{ kJ/mol}; \Delta U(\text{CPCM}) = -5 \text{ kJ/mol}$$

The solvent effect is very large, and results in a small thermodynamic stability of the six-coordinated intermediate. The slightly larger stability of $[UO_2(oxalate)_2(H_2O)_2]^{2-}$ over $[UO_2(oxalate)_2(H_2O)]^{2-}$ is below the accuracy of the quantum chemical methods used. In an EXAFS study to be reported[30] we have established that the $[UO_2(oxalate)_2]^{2-}$(aq) complex contains only one coordinated water.

(b) Water Exchange. The dissociative mechanism was studied following reaction 6 (Scheme 2) by progressively increasing the U−OH_2 distance in $[UO_2(ox)_2(H_2O)]^{2-}\cdot(H_2O)$ (Figure 8a). The activation energy $\Delta U^{\ddagger}$ was 21 and 56 kJ/mol, in the gas phase and solution, respectively, with the geometry of transition state and intermediate shown in Figure 8b,c. The energy difference between the transition state and the intermediate in the solvent, $\Delta U_I^{\ddagger}$, is small, 3 kJ/mol. The agreement between the dissociative model 10, without water in the second coordination sphere, and model 6 (Scheme 2) is good. In the transition state the leaving water is located outside the coordination plane, but returns to this plane in the intermediate, cf. Figure 8 b,c.

The transition state for the *A*- and *I*-pathways was investigated by stretching one or both of the U−OH_2 bonds in the intermediate $[UO_2(ox)_2(H_2O)_2]^{2-}$, Figure 9c. The water exchange can take place with the entering/leaving water molecules either in the trans or the cis position. It was only possible to

(29) Jayadevan, N. C.; Chackraburtty, D. M. *Acta Crystallogr.* **1972**, *B28*, 3178.
(30) Grenthe, et al. Unpublished results.

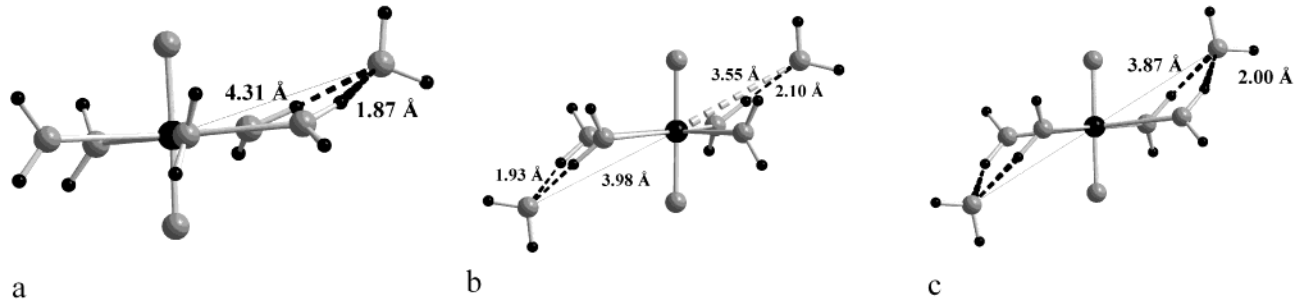

Figure 4. The *D*-mechanism for the uranyl(VI)−aqua ion. Perspective views of the reactant $[UO_2(H_2O)_5]^{2+}\cdot(H_2O)$ (a), the transition state $\{[UO_2(H_2O)_4\cdots(H_2O)]^{2+}\cdot(H_2O)\}^{\ddagger}$ (b), and the four-coordinated intermediate $[UO_2(H_2O)_4]^{2+}\cdot(H_2O)_2$ (c). The uranium atom and the hydrogen atoms are black and the oxygen atoms medium gray. The thin lines denote the distance between nonbonded atoms, the dark dashed lines hydrogen bond interactions. The light dashed bond denotes the leaving water in the transition state.

Table 3. Calculated Bond Distances and Point Group Assignment for the Species Participating in the Water Exchange Reaction[a]

chemical species	sym	figures	*d*(U−O) (Å)	H···O (Å)
$[UO_2(H_2O)_4]^{2+}$	D_{4h}	Figure S1	2.42, 2.42, 2.42, 2.42	
$[UO_2(H_2O)_5]^{2+}$ (reactant)	$\approx C_5$	Figure 2	2.46, 2.47, 2.47, 2.47, 2.48	
$\{[UO_2(H_2O)_4\cdots(H_2O)]^{2+}\}^{\ddagger}$ (*D*)	C_1	Figure S3b	2.42, 2.42, 2.43, 2.43, 3.60	1.84
$[UO_2(H_2O)_4]^{2+}\cdot(H_2O)$ (*D*-intermediate)	C_s	Figure S3c	2.43, 2.43, 2.44, 2.44, 4.04	1.90, 1.92
$[UO_2(H_2O)_5]^{2+}\cdot(H_2O)$ (reactant)	$\approx C_s$	Figure 1	2.46, 2.47, 2.47, 2.48, 2.49, 4.31	1.87, 1.88
$\{[UO_2(H_2O)_4\cdots(H_2O)]^{2+},(H_2O)\}^{\ddagger}$ (*D*)	C_1	Figure 4b	2.42, 2.43, 2.43, 2.44, 3.55, 3.99	1.93, 1.92, 2.10
$[UO_2(H_2O)_4]^{2+}\cdot(H_2O)_2$ (*D*-intermediate)	C_{2h}	Figure 4c	2.44, 2.44, 2.46, 2.46, 4.03, 4.03	1.97, 2.01, 1.97, 2.01
$\{[UO_2(H_2O)_5\cdots(H_2O)]^{2+}\}^{\ddagger}$ (*A*)	C_2	Figure 5b	2.47, 2.49, 2.49, 2.50, 2.54, 2.90	
$[UO_2(H_2O)_6]^{2+}$ (*A*-intermediate)	$\approx C_2$	Figure 5c	2.48, 2.48, 2.51, 2.51, 2.65, 2.65	
$\{[UO_2(H_2O)_4\cdots 2(H_2O)]^{2+}\}^{\ddagger}$ (*I*)	C_2	Figure 6b	gas-phase structure	gas-phase structure

[a] The geometry optimizations have been made without symmetry constraints at the HF level in the solvent (CPCM). H···O denotes the hydrogen bond distance between the water oxygen in the second coordination sphere and hydrogen atoms of the water in the first coordination sphere.

Table 4. HF and MP2 Energy Changes (ΔU, in kJ/mol) and Volume Changes (ΔV, in cm^3/mol) in the Solvent (CPCM) for *D*-, *A*-, and *I*-Mechanisms for Water Exchange in $[UO_2(H_2O)_5]^{2+}$ [a]

	CPCM geometry			gas-phase geometry
chemical species	ΔU(SCF) (kJ/mol)	ΔU(MP2) (kJ/mol)	ΔV (cm^3/mol)	ΔU(MP2) (kJ/mol)
$[UO_2(H_2O)_5]^{2+}$ (reactant)	0	0	0	
$\{UO_2(H_2O)_4\cdots(H_2O)]^{2+}\}^{\ddagger}$ (*D*)	50.9	59.2	+4.9	
$[UO_2(H_2O)_4]^{2+}$,(H_2O) (*D*-intermediate)	43.6	54.5	+3.6	
$[UO_2(H_2O)_5]^{2+}\cdot(H_2O))$ (reactant)	0	0	0	0
$\{[UO_2(H_2O)_4\cdots(H_2O)]^{2+}\cdot(H_2O)\}^{\ddagger}$ (*D*)	62.0	74.0	+4.6	70.1
$[UO_2(H_2O)_4]^{2+}\cdot(H_2O)_2$ (*D*-intermediate)	53.7	61.8	+4.2	65.8
$\{[UO_2(H_2O)_5\cdots(H_2O)]^{2+}\}^{\ddagger}$ (*A*)	21.0	18.7	−3.0	
$[UO_2(H_2O)_6]^{2+}$ (*A*-intermediate)	20.8	15.8	−3.4	
$\{[UO_2(H_2O)_4\cdots 2(H_2O)]^{2+}\}^{\ddagger}$ (*I*)				21.2

[a] Column 5 refers to single-point MP2 calculations in the solvent using the gas phase geometry, cf. Table 1. The experimental activation parameters are $\Delta H^{\ddagger} = 26 \pm 1$ kJ/mol and $\Delta S^{\ddagger} = -40 \pm 5$ J/(mol·K).

identify transition states and intermediates in the trans case. The activation energy for the *A*-mechanism is $\Delta U^{\ddagger} = 29$ and 12 kJ/mol, in the gas phase and solvent models, respectively, with the geometry of the transition state shown in Figure 9b. The distances between U and the entering and leaving water in the transition state are 2.62 and 3.00 Å, respectively. The energy difference, $\Delta U_I^{\ddagger}$, between the intermediate and the transition state in the *A*-mechanism is 16 kJ/mol, resulting in a lifetime for the intermediate of $\approx 10^{-8}$ s as estimated by the relationship

$$\tau = \frac{1}{Z}\exp\{\Delta U_I^{\ddagger}/RT\};\ Z \approx 10^{11}\ s^{-1} \qquad (15)$$

which is probably too short to be noticed experimentally.

The *I*-mechanism has an activation energy $\Delta U^{\ddagger} = 53$ kJ/mol, significantly larger than that for the *A*-mechanism and close to the value found for the *D*-mechanism. The distance between uranium and the entering/leaving water in the *I*-transition state is 3.10 Å, cf. Figure 10b, slightly shorter than in the *D*-mechanism, indicating that it is of I_d-type.

(c) Conclusion. Based on the comparison of the activation energies, the water exchange in the oxalate system follows an associative pathway. The corresponding activation energy is not significantly different from that found in the $[UO_2(H_2O)_5]^{2+}$ system.

Discussion

The Accuracy of the Model. (a) Methods Used. First a general comment on the methods used, as already mentioned in the Introduction, the various structures have been studied at the Hartree−Fock level, with energies calculated at the MP2 level. A previous study[5] showed that correlation had only a small effect on the uranium−ligand bond distances in the equatorial plane—the largest effect was observed in the internal uranyl bond distance. There is a general tendency of the quantum chemical method to give uranium−water distances that are up to 0.1 Å[5,24] longer than the experimental values. This is a systematic error and we can therefore assume that it is constant along the reaction pathway.

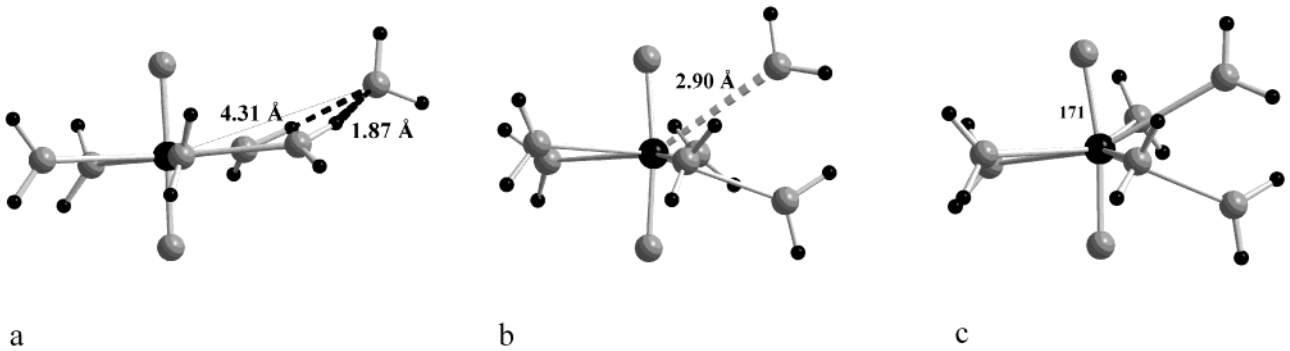

Figure 5. The *A*-mechanism for the uranyl(VI)−aqua ion. Perspective views of the reactant $[UO_2(H_2O)_5]^{2+}\cdot(H_2O)$ (a), transition state $\{[UO_2(H_2O)_5\cdots(H_2O)]^{2+}\}^{\ddagger}$ (b) and the six-coordinated intermediate $[UO_2(H_2O)_6]^{2+}$ (c). The uranium atom and the hydrogen atoms are black and the oxygen atoms medium gray. The thin lines denote the distance between nonbonded atoms, the dark dashed lines hydrogen bond interactions. The light dashed bond denotes the leaving water in the transition state.

Table 5. Calculated Bond Distances and Point Group Assignment for the Water Exchange Reaction in the Uranyl Oxalate Ion $[UO_2(C_2O_4)_2(H_2O)]^{2-}$ [a]

chemical species	sym	figures	*d*(U−O) (Å)	H···O (Å)
$[UO_2(C_2O_4)_2]^{2-}$	$\approx D_{2h}$	Figure S4	2.33, 2.35, 2.36, 2.39	
$[UO_2(C_2O_4)_2(H_2O)]^{2-}$ (reactant)	C_s	Figure 7	2.36, 2.36, 2.42, 2.42, 2.62	
$\{[UO_2(C_2O_4)_2\cdots(H_2O)]^{2-}\}^{\ddagger}$ (*D*)	$\approx C_s$	Figure S5b	2.35, 2.35, 2.38, 2.39, 3.20	1.90, 1.92
$[UO_2(C_2O_4)_2]^{2-}\cdot(H_2O)$ (*D*-intermediate)	$\approx C_s$	Figure S5c	2.34, 2.35, 2.38, 2.38, 5.48	1.97
$[UO_2(C_2O_4)_2(H_2O)]^{2-}\cdot(H_2O)$ (reactant)	C_1	Figure 8a	2.35, 2.38, 2.41, 2.42, 2.61, 5.48	1.96
$\{[UO_2(C_2O_4)_2\cdots(H_2O)]^{2-}\cdot(H_2O)\}^{\ddagger}$ (*D*)	C_1	Figure 8b	2.34, 2.35, 2.36, 2.39, 3.45, 5.47	1.93, 1.97
$[UO_2(C_2O_4)_2]^{2-}\cdot(H_2O)_2$ (*D*-intermediate)	C_{2h}	Figure 8c	2.35, 2.35, 2.37, 2.37, 5.48, 5.48	1.97, 1.97
$\{[UO_2(C_2O_4)_2(H_2O)\cdots(H_2O)]^{2-}\}^{\ddagger}$ (*A*)	C_s	Figure 9b	2.42, 2.42, 2.44, 2.44, 2.62, 3.00	2.03, 2.03
$[UO_2(C_2O_4)_2(H_2O)_2]^{2-}$ (*A*-intermediate)	C_{2h}	Figure 9c	2.45, 2.45, 2.45, 2.45, 2.67, 2.67	-
$\{[UO_2(C_2O_4)_2\cdots 2(H_2O)]^{2-}\}^{\ddagger}$ (*I*)	C_{2v}	Figure 10b	2.40, 2.40, 2.40, 2.40, 3.10, 3.10	2.10, 2.10

[a] The geometry opimizations have been made without symmetry constraints at the HF level in the gas phase. H···O denotes the hydrogen bond distance between the water oxygen in the second coordination sphere and hydrogen atoms of the water in the first coordination sphere.

Table 6. HF and MP2 Energy Changes (in kJ/mol) and Volume Changes (in cm^3/mol) in the Solvent (CPCM) for *D*-, A,- and *I*-Mechanisms for Water Exchange in $[UO_2(C_2O_4)_5(H_2O)]^{2-}$, Calculated in the Gas Phase and in the Solvent (CPCM) Using the Gas-Phase Geometry

chemical species	ΔU(SCF) (kJ/mol) gas phase	ΔU(MP2) (kJ/mol) gas phase	ΔU(MP2) (kJ/mol) CPCM	ΔV (cm^3/mol)
$[UO_2(C_2O_4)_2(H_2O)]^{2-}$ (reactant)	0	0	0	0
$\{[UO_2(C_2O_4)_2\cdots(H_2O)]^{2-}\}^{\ddagger}$ (*D*)	14.5	20.6	53.8	4.6
$\{[UO_2(C_2O_4)_2]^{2-}\cdot(H_2O)$ (*D*-intermediate)	−11.1	3.8	53.0	4.6
$[UO_2(C_2O_4)_2(H_2O)]^{2-}\cdot(H_2O)$ (reactant)	0	0	0	0
$\{[UO_2(C_2O_4)_2\cdots(H_2O)]^{2-}\cdot(H_2O)\}^{\ddagger}$ (*D*)	13.7	21.3	56.3	4.1
$[UO_2(C_2O_4)_2]^{2-}\cdot(H_2O)_2$ (*D*-intermediate)	−7.5	8.0	53.5	4.0
$\{[UO_2(C_2O_4)_2(H_2O)\cdots(H_2O)]^{2-}\}^{\ddagger}$ (*A*)	35.8	28.8	11.7	−3.5
$[UO_2(C_2O_4)_2(H_2O)_2]^{2-}$ (*A*-intermediate)	34.0	24.9	−4.6	−6.3
$\{[UO_2(C_2O_4)_2\cdots 2(H_2O)]^{2-}\}^{\ddagger}$ (*I*)	42.9	40.6	53.2	−0.3

Correlation affects the energy of the ground state, the transition state, and the intermediates in different ways, resulting in an increase in the activation energy for the *D*-mechanism and a decrease in activation energy for the *A/I*-mechanisms, and corresponding energy changes in the intermediates, cf. Tables 2 and 4. However, correlation effects are moderate, at most 12 kJ/mol.

Recently, Tsushima et al.[31] have studied uranyl coordinated by five and six water molecules in the gas phase and solution, using B3LYP, large core ECPs, and the PCM model. It appears that the geometries have been optimized with symmetry constraints. There are a number of significant discrepancies between our results and theirs. Our experience is that it is important to relax symmetry constraints wherever possible, and we believe the symmetry constraints imposed by Tsushima et al. to be one important reason for the differences observed. Another factor may be that they are using a larger core than we do. We have found that it is important to keep a small core; in a test calculation on reduction of uranyl,[32] the large core ECP included in Gaussian98 gave a reaction energy that was about 20 kJ/mol more endothermic than that obtained with the small core ECPs used by us (35 vs 16 kJ/mol).

(b) Activation Parameters. The experimental data provide information on $\Delta H^{\ddagger}$ and $\Delta S^{\ddagger}$ at 298 K. The quantum chemical models used here give a static picture (at 0 K) of the energy and geometry changes along a particular reaction pathway. Following the arguments of Katakis and Gordon[33] we assume that $\Delta U^{\ddagger}(0K) \approx \Delta U^{\ddagger}(298K)$. These two quantities differ by the change in thermal energy $\int C_v^{\ddagger}\,dT - \int C_v\,dT$, where C_v and $C_v^{\ddagger}$ are the molar heat capacity in the initial and transition states, respectively. This difference should in general be small; as an example it amounts to 2 J/K/mol for reaction 9 as obtained in

(31) Tsushima, S.; Yang, T.; Suzuki, A. *Chem. Phys. Lett.* **2001**, *334*, 365.

(32) Vallet, V.; Maron, L.; Schimmelpfennig, B.; Leininger, T.; Teichteil, C.; Gropen, O.; Grenthe, I.; Wahlgren, U. *J. Phys. Chem A* **1999**, *103*, 9285.

(33) Katakis, D.; Gordon, G. *Mechanisms of inorganic reactions*; Wiley & Sons: New York, 1987.

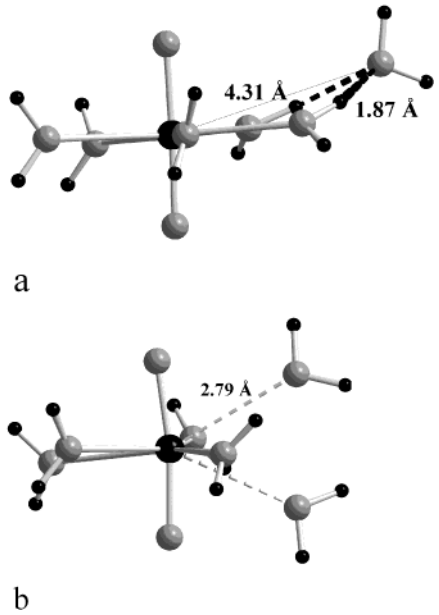

Figure 6. The *I*-mechanism for the uranyl(VI)−aqua ion. Perspective views of the reactant $[UO_2(H_2O)_5]^{2+}\cdot(H_2O)$ (a) and symmetric transition state $\{[UO_2(H_2O)_4\cdots(H_2O)_2]^{2+}\}^{\ddagger}$ (b). The uranium atom and the hydrogen atoms are black and the oxygen atoms medium gray. The thin lines denote the distance between nonbonded atoms, the dark dashed lines hydrogen bond interactions. The light dashed bond denotes the leaving water in the transition state.

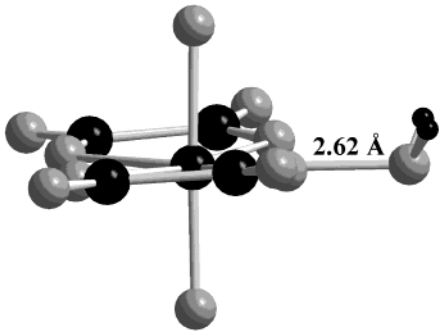

Figure 7. Perspective view of $[UO_2(C_2O_4)_2(H_2O)]^{2-}$. The uranium atom, the carbon atoms, and the hydrogen atoms are black and the oxygen atoms medium gray.

Gaussian98. The correction for zero-point energy, which affects $\Delta U^{\ddagger}$ should be small in our case, as no covalent bonds are broken or formed. Furthermore, we have $\Delta H = \Delta U + \Delta(PV) \approx \Delta U$ for reactions in solution. Hence $\Delta U^{\ddagger}(0K) \approx \Delta H^{\ddagger}(298K)$ seems to be a reasonable approximation.

The quantum chemical methods allow the calculation of $\Delta S^{\ddagger}$ that can be compared with experimental data. However, the calculated quantity is strongly model dependent, being based on the harmonic approximation for the calculation of vibration energy levels, and in addition not taking rotation energy levels into account. Furthermore, by using a homogeneous solvent model without a full second coordination sphere it is not possible to take full account of the entropy contribution originating from molecular interactions between the first coordination sphere and the solvent.[34] For these reasons we have not used $\Delta S^{\ddagger}$ as a mechanistic indicator.

(c) The Solvent Model. The first quantum chemical investigations of water exchange mechanisms were made by using a gas-phase model.[6,7,12,13] This model was justified by the good agreement between calculated and measured activation energies. However, this was probably fortuitous, since Rotzinger[8] in a later study noticed that the solvent model had an important effect on the activation parameters that even led to changes in the preferred reaction pathway. The shape of the cavity has a large effect on the estimation of the hydration energy as discussed previously.[5,35] A spherical cavity may be appropriate for highly symmetric octahedral complexes, but not for those with a pronounced nonspherical shape,[5,36] for which the cavity volume is significantly overestimated, cf. Table 5 of ref 36. We have therefore used the CPCM model with shape-adapted cavity in our calculations. The uranium radius used to build the cavity has been taken from the standard database in Gaussian98. However, Barone et al.[22] found that fine tuning of the metal radii was essential to accurately reproduce the experimental solvation free energy. This adjustment cannot be performed for actinides as such data are not available. Nevertheless, we checked how the reaction energy for eq 9 is affected by a change of the radius of uranium from 1.86 to 1.74 Å. This was 10 kJ mol and the change for reactions (3), (4) and (5) of Scheme 1 are expected to be smaller and insignificant for the mechanistic conclusions.

The main contribution to the hydration energy comes from the electrostatic interactions, which decrease with increasing cavity volume. Clearly, the solvent effect along the reaction pathways is not the same for the transition state/intermediate and the reactants. The general conclusion supported by our calculations is an increase of the activation barrier for the *D*-mechanisms and a decrease for the *A/I*-mechanisms which is consistent with the larger cavity volume in the transition state for the *D*-mechanism. This is also in agreement with the results from Rotzinger[8] showing a decrease in the activation energy of about 20 kJ/mol for an *A/I*-mechanisms as compared to the gas phase, and an increase of about 20 kJ/mol for a *D*-mechanism for water exchange in octahedral complexes. Hartmann et al.[12] observed that the computed activation energy in the gas phase for an *A*-pathway was larger than the experimental value and suggested that this difference might be due to solvent effects; the discussion above indicates that this is correct. The results presented above indicate that it is possible to estimate the effect of solvation for different reaction mechanisms.

Solvent effects induce a general shortening of the uranium−ligand bond, the effect being small: 0.04−0.06 Å for the spectator ligands and larger for the distances to the entering/leaving water molecule. Single-point calculations at the optimized gas-phase structure seem to provide a good estimate of the effects of hydration, as shown by the results on the uranyl aqua ion, cf. Table 4. The reason is that the potential surface is shallow around the transition state and intermediate, as noticed in the calculations. This is an important finding because it allows the estimation of solvent effects also in systems where a complete geometry optimization would be both complex and expensive, as is the case for the U(VI) oxalate complexes.

The Water Exchange. The large difference between the first coordination spheres in $[UO_2(H_2O)_5]^{2+}$ and $[UO_2(oxalate)_2(H_2O)]^{2-}$ will affect their second coordination spheres and possibly also the rate and mechanism of water exchange. The quantum chemical results indicate a change from an *I/A*-mechanism in $[UO_2(H_2O)_5]^{2+}$ to a pure *A*-mechanism in $[UO_2(oxalate)_2(H_2O)]^{2-}$, but no large change in activation energy. There is no direct experimental information on the water

(34) Searle, M. S.; Williams, D. H. *J. Am. Chem. Soc.* **1992**, *114*, 10690.

(35) Tomasi, J.; Persico, M. *Chem. Rev.* **1994**, *94*, 2027.

(36) Foresman, J. B.; Keith, T. A.; Wiberg, K. B.; Soonian, J.; Frisch, M. J. *J. Phys. Chem.* **1996**, *100*, 16098.

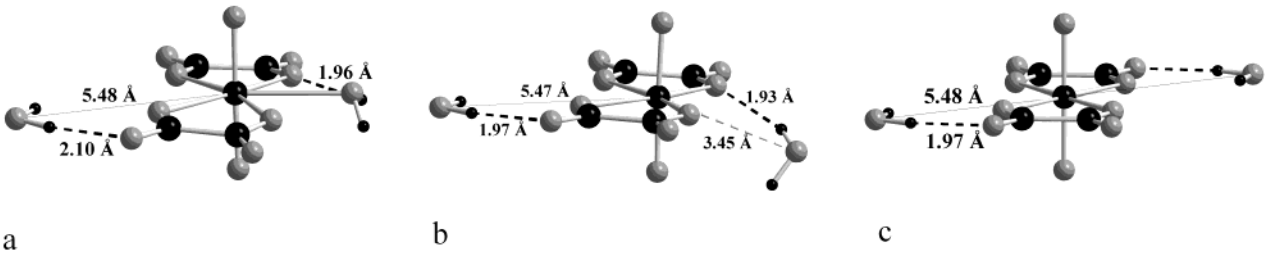

Figure 8. The *D*-mechanism for the uranyl(VI)−oxalate complex. Perspective views of the reactant $[UO_2(C_2O_4)_2(H_2O)]^{2-}\cdot(H_2O)$ (a), transition state $\{[UO_2(C_2O_4)_2\cdots(H_2O)]^{2-}\cdot(H_2O)\}^{\ddagger}$ (b), and four-coordinated intermediate $[UO_2(C_2O_4)_2]^{2-}\cdot(H_2O)_2$ (c). The uranium atom, the carbon atoms, and the hydrogen atoms are black and the oxygen atoms medium gray. The thin lines denote the distance between nonbonded atoms, the dashed lines hydrogen bond interactions.

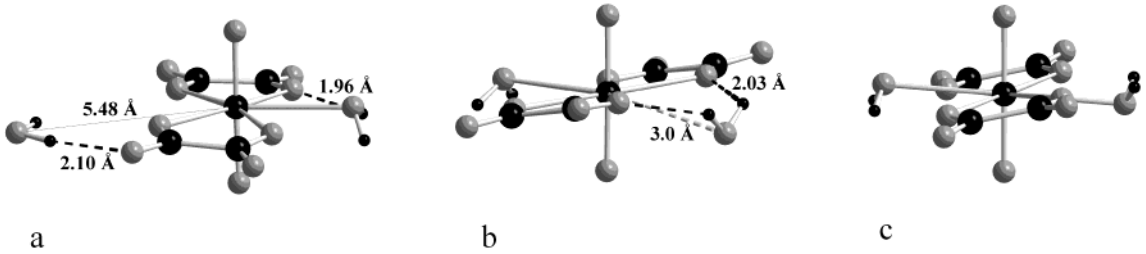

Figure 9. The *A*-mechanism for the uranyl(VI)-oxalate complex. Perspective views of the reactant $[UO_2(C_2O_4)_2(H_2O)]^{2-}\cdot(H_2O)$ (a), transition state $\{[UO_2(C_2O_4)_2(H_2O)\cdots(H_2O)]^{2-}\}^{\ddagger}$ (b), and six-coordinated intermediate $[UO_2(C_2O_4)_2(H_2O)_2]^{2-}$ (c). The uranium atom, the carbon atoms, and the hydrogen atoms are black and the oxygen atoms medium gray. The thin lines denote the distance between nonbonded atoms, the dashed lines hydrogen bond interactions.

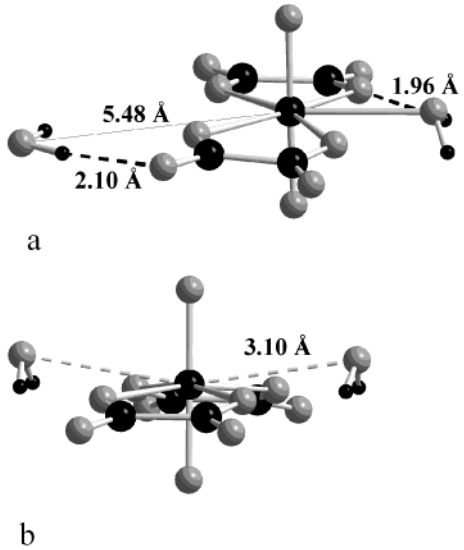

Figure 10. The *I*-mechanism for the uranyl(VI)−oxalate complex. Perspective views of the reactant $[UO_2(C_2O_4)_2(H_2O)]^{2-}\cdot(H_2O)$ (a) and transition state $\{[UO_2(C_2O_4)_2\cdots(H_2O)_2]^{2-}\}^{\ddagger}$ (b). The uranium atom, the carbon atoms, and the hydrogen atoms are black and the oxygen atoms medium gray. The thin lines denote the distance between nonbonded atoms, the dashed lines hydrogen bond interactions.

exchange for the oxalate system, only indirect evidence from the experimental rate law for the oxalate exchange reaction:[37]

$$[UO_2(ox)_2(H_2O)]^{2-} + [*ox]^{2-} \rightleftharpoons [UO_2(*ox)_2(H_2O)]^{2-} + [ox]^{2-}$$

with $v = k_{exp}[UO_2(ox)_2(H_2O)^{2-}][ox^{2-}]$. This second-order rate law is consistent with a mechanism where the first step is the rapid formation of an outer-sphere complex, followed by a rate-determining release of water. The experimental activation energy, $\Delta H^{\ddagger} = 31$ kJ/mol,[37] is very close to that for water-exchange in $[UO_2(H_2O)_5]^{2+}$, $\Delta H^{\ddagger} = 26$ kJ/mol,[15] and in fair agreement with the calculated activation energy for the *A*-mechanism in $[UO_2(oxalate)_2(H_2O)]^{2-}$, $\Delta U^{\ddagger} = 12$ kJ/mol.

The structures of the transition state in the *I/A*-mechanisms and the intermediate in the *A*-mechanism clearly show that the "yl" oxygens in uranium(VI) do not prevent the entry of ligands from above and below the coordination plane. This is important, especially when using uranium(VI) complexes as templates and/or catalysts in organic synthesis.

Conclusion

A comparison of the experimental activation energy $\Delta H^{\ddagger}$(298K) with the theory based quantity $\Delta U^{\ddagger}$(0K) and the geometry of reactants, transition states, and intermediates for the reactions studied here provide strong evidence that the water exchange in $[UO_2(H_2O)_5]^{2+}$ takes place through an *A*- or *I*-mechanism. The difference between the two pathways is small, indicating that it will not be possible to distinguish between them experimentally. This is also in agreement with the relatively low experimental value of $\Delta H^{\ddagger} = 26$ kJ/mol and the negative $\Delta S^{\ddagger} = -40$ J/(K·mol). In $[UO_2(ox)_2(H_2O)]^{2-}$ the water exchange seems to follow a pure *A*-mechanism, with an activation energy similar to that for the pentaaqua complex. The dissociative pathway for the water exchange in $[UO_2(H_2O)_5]^{2+}$ has a much higher activation energy than those for the *A/I*-mechanisms and can safely be excluded. In the same way, the *D/I*-pathways in $[UO_2(ox)_2(H_2O)]^{2-}$ can be excluded because their activation energies are much larger that that for the *A*-mechanism.

Acknowledgment. This study has been supported by a generous grant from the Carl Trygger Foundation. We would also like to acknowledge the support of the French Cotutelle program, as well as the computer resources provided by the University of Tromsø.

(37) Aas, W.; Szabó, Z.; Grenthe, I. *J. Chem. Soc., Dalton Trans.* **1999**, 1311.

Supporting Information Available: All the structures not presented in the text (Figures S1−S5) and the coordinates and total energies of all computed structures (Tables S1−S3) (PDF). This material is available free of charge via the Internet at http://pubs.acs.org.

JA015935+